Dyes and Pigments 200 (2022) 110125

Contents lists available at ScienceDirect

Dyes and Pigments

journal homepage: www.elsevier.com/locate/dyepig

New metallophthalocyanines including benzylphenoxy groups and investigation of their organic-field effect transistor (OFET) features

Mücahit Özdemir [a], Sinem Altinisik [b], Baybars Köksoy [c,*], Betül Canımkurbey [d,e], Sermet Koyuncu [b], Mahmut Durmuş [f], Mustafa Bulut [a], Bahattin Yalçın [a]

[a] Marmara University, Department of Chemistry, 34722, Istanbul, Turkey
[b] Çanakkale Onsekiz Mart University, Department of Chemical Engineering, 17400, Çanakkale, Turkey
[c] Bursa Technical University, Department of Chemistry, 16310, Bursa, Turkey
[d] Amasya University, Sabuncuoglu Şerefeddin Health Services Vocational School, 05100, Amasya, Turkey
[e] Amasya University, Central Research Laboratory, 05100, Amasya, Turkey
[f] Gebze Technical University, Department of Chemistry, 41400, Kocaeli, Turkey

ARTICLE INFO

Keywords:
Synthesis
Phthalocyanine
Electrochemistry
OFET
DFT

ABSTRACT

In this study, metal and metal-free novel phthalocyanines containing peripheral and non-peripheral tetra 2-benzylphenoxy groups were synthesized. The compounds were characterized by UV–Vis, FT-IR, ^{1}H NMR, and MALDI-TOF mass spectrometry as well as elemental analysis. These new phthalocyanines exhibited excellent solubility in most organic solvents, and their redox behavior was investigated in different solvents such as dimethyl sulfoxide (DMSO) and dichloromethane (DCM). The redox behavior of the peripheral and non-peripheral phthalocyanine compounds **1a-c** and **2a-c** was determined by cyclic voltammetry and *in situ* spectroelectrochemistry. According to organic field-effect transistors (OFETs) measurements, the peripheral and non-peripheral phthalocyanine-cobalt complexes which have higher mobility than others were utilized top-gate bottom-contact OFETs fabrication. The output characteristics of the device show that its mobility is approximately 5×10^{-2} cm^2/Vs with p-type accumulation.

1. Introduction

Phthalocyanines which include diiminoisoindoline units are a class of pigments family in organic chemistry. These macrocycles have an 18-π electron system, green-blue color, and chemical-physical stability. In recent years, after the discovery of the phthalocyanine macrocycle, many studies have been made in the literature on these compounds. Their applications in many areas have been revealed by using the optical, physical, and electrochemical properties of phthalocyanines. Some application fields of phthalocyanines are photodynamic therapy [1,2], electronic and optoelectronic applications [3–5], catalysts [6,7], liquid crystals [8–10], and sensors [11,12].

The feasibility of these areas including electrocatalysis, electrochromism, and energy-producing devices is bound to their excellent electron transfer properties. Therefore, the determination of the electrochemical features of novel metallophthalocyanines (MPcs) has vital importance in identification to the possibility of these usages in technological applications.

The alignment of MPcs molecules to columnar molecular clusters is achieved by the overlap between π-orbitals of adjacent molecules. As a result of this alignment, one-dimensional wires are formed surrounded by an insulating layer produced by aliphatic chains. Such films with a columnar structure feature anisotropic charge-bearing mobility [13,14]. Their usage in the application areas given above is a result of the electronic character that these features have added to the structure. For these mentioned applications, the regular structure, and smooth surfaces of MPcs films play an important role in obtaining devices by improved performance [15]. The specifications such as operating voltage and field-effect mobility used to identify an OFET are controlled by the reliability of the gate insulator and the density of charge traps at the dielectric-semiconductor interface. Therefore, it is important to develop a suitable gate dielectric with high capacitance and low leakage current to achieve the desired OFET performance [16].

Herein, benzyl phenoxy substituted phthalocyanines were synthesized by cyclotetramerization of phthalonitrile derivatives. After characterizing the compounds with various methods, the molecular energy

* Corresponding author.
E-mail address: baybars.koksoy@btu.edu.tr (B. Köksoy).

https://doi.org/10.1016/j.dyepig.2022.110125
Received 12 October 2021; Received in revised form 14 January 2022; Accepted 21 January 2022
Available online 30 January 2022
0143-7208/© 2022 Elsevier Ltd. All rights reserved.

levels, and oxidation/reduction behavior of MPcs were determined by density functional theory (DFT) calculations. Besides the optical and electrical properties of the structures, contact angle values and surface morphologies of thin films were investigated. It is aimed to use MPcs in OFET applications due to their large charge carrier mobility as well as their large exciton diffusion lengths along with the axis of columnar stacks. Finally, the usage of MPc in OFET applications due to their high load-bearing mobility and their large exciton diffusion lengths along the axis of columnar stacks were investigated.

2. Experimental

Material, methods, equipment details, and some characterization parameters were provided in the supporting information.

2.1. Synthesis

The compounds **1** and **2** were synthesized by nucleophilic aromatic substitution and benzyl phenoxy substituted phthalocyanines (**1a-c**/**2a-c**) were synthesized by cyclotetramerization of phthalonitrile derivatives (**1**, **2**) according to the procedure given in the literature [17].

2.1.1. General synthesis procedure for phthalonitriles (1–2)

2-Benzylphenol (1 g, 5.43 mmol) and 4-nitrophthalonitrile/3-nitrophthalonitrile compounds (0.94 g, 5.43 mmol) were stirred in 25 mL anhydrous DMF. After stirring, anhydrous K_2CO_3 was slowly added to the reaction. The mixture was stirred at 60–65 °C for 48 h. At the end of this time, the reaction mixture was poured into ice water, then filtered and dried. The crude product was purified by column chromatography on silica gel using chloroform as eluent.

2.1.1.1. 4-(2-Benzyl phenoxy) phthalonitrile (1). Yield: 1.23 g (73.2%), m.p.: 265–267 °C. Anal. Calc. For [$C_{21}H_{14}N_2O$] (Mw: 310.36 g/mol): C, 81.27; H, 4.55; N, 9.03%, found: C, 81.25; H, 4.53; N, 9.01%. FT-IR (ATR): ν_{max}, cm^{-1} 3026 (Aromatic C–H), 2910–2872 (Aliphatic C–H), 2232 (–C≡N), 1598–1480 (Aromatic C=C), 1248 (Ar–O–Ar). ^{1}H NMR ($CDCl_3$, δ, ppm) 7.60 (d, J = 8.6 Hz, 1H), 7.41 (d, J = 7.9 Hz, 1H), 7.36–7.31 (m, 2H), 7.17–7.13 (m, 3H), 7.06–7.04 (m, 3H), 6.99 (d, J = 7.9 Hz, 1H), 6.96 (s, 1H), 3.91 (s, 2H). ^{13}C NMR ($CDCl_3$, δ, ppm) 161.65, 151.49, 139.09, 135.09, 133.85, 132.23, 128.81, 128.75, 128.45, 126.79, 126.36, 121.41, 120.72, 120.69, 117.35, 115.44, 114.93, 108.32 and 36.52.

2.1.1.2. 3-(2-Benzyl phenoxy) phthalonitrile (2). Yield: 1.08 g (64.1%), m.p.: 278–280 °C. Anal. Calc. For [$C_{21}H_{14}N_2O$] (Mw: 310.36 g/mol): C, 81.27; H, 4.55; N, 9.03%, found: C, 81.26; H, 4.50; N, 9.02%. FT-IR (ATR): ν_{max}, cm^{-1} 3026 (Aromatic C–H), 2919–2846 (Aliphatic C–H), 2231 (–C≡N), 1596–1483 (Aromatic C=C), 1249 (Ar–O–Ar). ^{1}H NMR ($CDCl_3$, δ, ppm) 7.40 (d, J = 8.5 Hz, 1H), 7.34–7.28 (m, 4H), 7.17–7.07 (m, 5H), 7.00 (d, J = 7.8 Hz, 1H), 6.65 (m, 1H), 3.98 (s, 2H). ^{13}C NMR ($CDCl_3$, δ, ppm) 160.78, 151.51, 139.17, 134.02, 133.95, 132.08, 128.91, 128.48, 128.42, 126.68, 126.44, 126.23, 121.17, 119.37, 116.88, 115.20, 112.74, 105.21 and 36.56.

2.1.2. General synthesis procedure for phthalocyanine compounds (1a-c/2a-c)

A mixture of phthalonitrile compounds **1** or **2** (0.100 g, 0.32 mmol) and metal salts [$CuCl_2$, $NiCl_2$, $CoCl_2$, (0.025 g, 0.19 mmol)] in *N,N*-dimethylaminoethanol (3 mL) were stirred at 160 °C for 22 h under argon atmosphere. After cooling to room temperature, the reaction mixture was poured into the water to precipitate the blue-green product. This crude product was washed several times with different solvents such as hot water, hot acetic acid, methanol and purified by column chromatography on silica gel using chloroform as an eluent.

2.1.2.1. ***2(3),9(10),16(17),23(24)-Tetrakis[2-benzylphenoxy] phthalocyaninato copper (II) (1a)***. Yield: 0.050g (47.6%), m.p.: >300 °C. Anal. Calc. For [$C_{84}H_{56}N_8O_4Cu$]: C, 77.31; H, 4.33; N, 8.59%, found: C, 77.29; H, 4.30; N, 8.57%. UV–Vis (Dichloromethane): λ_{max} nm (log ε) 339 (4.82), 614 (4.54), 683 (5.19). FT-IR (ATR): ν_{max}, cm^{-1} 3027 (Aromatic C–H), 2956–2868 (Aliphatic C–H), 1582–1469 (Aromatic C=C), 1230 (Ar–O–Ar). MALDI-TOF-MS *m/z*: calc. 1304.97; found 1305.13 $[M]^+$.

2.1.2.2. ***2(3),9(10),16(17),23(24)-Tetrakis[2-benzylphenoxy] phthalocyaninato nickel (II) (1b)***. Yield: 0.036g (34.3%), m.p.: >300 °C. Anal. Calc. For [$C_{84}H_{56}N_8O_4Ni$]: C, 77.60; H, 4.34; N, 8.62%, found: C, 77.56; H, 4.33; N, 8.58%. UV–Vis (Dichloromethane): λ_{max} nm (log ε) 351 (4.80), 614 (4.46), 682 (5.19). FT-IR (ATR): ν_{max}, cm^{-1} 3028 (Aromatic C–H), 2933–2867 (Aliphatic C–H), 1597–1483 (Aromatic C=C), 1248 (Ar–O–Ar). MALDI-TOF-MS *m/z*: calc. 1300.12; found 1300.06 $[M]^+$.

2.1.2.3. ***2(3),9(10),16(17),23(24)-Tetrakis[2-benzylphenoxy] phthalocyaninato cobalt (II) (1c)***. Yield: 0.053g (50.5%), m.p.: >300 °C. Anal. Calc. For [$C_{84}H_{56}N_8O_4Co$]: C, 77.59; H, 4.34; N, 8.62%, found: C, 77.55; H, 4.32; N, 8.60%. UV–Vis (Dichloromethane): λ_{max} nm (log ε) 330 (4.91), 610 (4.59), 675 (5.19). FT-IR (ATR): ν_{max}, cm^{-1} 3026 (Aromatic C–H), 2945–2878 (Aliphatic C–H), 1582–1449 (Aromatic C=C), 1229 (Ar–O–Ar). MALDI-TOF-MS *m/z*: calc. 1300.36; found 1300.16 $[M]^+$.

2.1.2.4. ***1(4),8(11),15(18),22(25)-Tetrakis[2-benzylphenoxy] phthalocyaninato copper (II) (2a)***. Yield: 0.043g (41.0%), m.p.: >300 °C. Anal. Calc. For [$C_{84}H_{56}N_8O_4Cu$]: C, 77.31; H, 4.33; N, 8.59%, found: C, 77.29; H, 4.30; N, 8.57%. UV–Vis (Dichloromethane): λ_{max} nm (log ε) 327 (4.53), 631 (4.42), 703 (5.13). FT-IR (ATR): ν_{max}, cm^{-1} 3027 (Aromatic C–H), 2929–2858 (Aliphatic C–H), 1576–1451 (Aromatic C=C), 1246 (Ar–O–Ar). MALDI-TOF-MS *m/z*: calc. 1304.97; found 1304.15 $[M]^+$.

2.1.2.5. ***1(4),8(11),15(18),22(25)-Tetrakis[2-benzylphenoxy] phthalocyaninato nickel (II) (2b)***. Yield: 0.038g (36.2%), m.p.: >300 °C. Anal. Calc. For [$C_{84}H_{56}N_8O_4Ni$]: C, 77.60; H, 4.34; N, 8.62%, found: C, 77.56; H, 4.33; N, 8.58%. UV–Vis (Dichloromethane): λ_{max} nm (log ε) 331 (4.96), 630 (4.45), 700 (5.20). FT-IR (ATR): ν_{max}, cm^{-1} 3028 (Aromatic C–H), 2930–2866 (Aliphatic C–H), 1586–1488 (Aromatic C=C), 1267 (Ar–O–Ar). MALDI-TOF-MS *m/z*: calc. 1300.12; found 1300.06 $[M]^+$.

2.1.2.6. ***1(4),8(11),15(18),22(25)-Tetrakis[2-benzylphenoxy] phthalocyaninato cobalt (II) (2c)***. Yield: 0.048g (45.7%), m.p.: >300 °C. Anal. Calc. For [$C_{84}H_{56}N_8O_4Co$]: C, 77.59; H, 4.34; N, 8.62%, found: C, 77.55; H, 4.32; N, 8.60%. UV–Vis (Dichloromethane): λ_{max} nm (log ε) 319 (4.75), 623 (4.49), 690 (5.13). FT-IR (ATR): ν_{max}, cm^{-1} 3027 (Aromatic C–H), 2936–2876 (Aliphatic C–H), 1578–1449 (Aromatic C=C), 1246 (Ar–O–Ar). MALDI-TOF-MS *m/z*: calc. 1300.36; found 1300.09 $[M]^+$.

2.2. Computational parameters

Optimized molecular geometries and molecular properties of the novel phthalocyanines (**1a-c** and **2a-c**) were determined using Density Functional Theory (DFT) [18]. Molecular structures of investigated phthalocyanines were optimized by Gaussian09 [19] in dichloromethane (DCM) and visualized by GaussView 5.0 [20]. For DFT, the hybrid B3LYP functional (B3: Becke's three-parameter nonlocal exchange functional [21,22], LYP: Lee-Yang-Parr's correlation function [23]) were used with the GEN basis set, 6-31G(d,p) for C, H, O, N atoms and LANL2DZ for central metals (Cu, Ni, Co) was chosen. The solvent

effect was investigated using the Polarizable Continuum Model (PCM) [24,25] in the ground state as implemented in Gaussian09. To compare the experimental and theoretical UV–Vis absorption spectra, the time-dependent DFT method was used to measure the UV–Vis absorption spectra by B3LYP using the same basis sets in dichloromethane (DCM). Total SCF density mapped with the electrostatic potential was visualized at 0.02 isovalues and 0.0004 e/au^3 isodensity value for a presentation of the charge distributions and reactive site of the molecules.

2.3. OFET fabrication

Au source/drain electrodes with 30 mm channel width and 50 μm channel length on glass substrate were obtained by a lithography method. After the Au electrode deposition, the phthalocyanine layer is spin-coated and then only the PMMA layer is created. Therefore, the dielectric constant of the PMMA dielectric layer (Ɛ) is around 3.6 at 100Hz. Then polymethyl methacrylate (PMMA) was coated onto the phthalocyanine layer at 1500 rpm. Phthalocyanines (**1a-c and 2a-c**) were coated by the spin coating method at 1000 rpm. Aluminum was evaporated on the PMMA layer as a gate electrode (~100 nm). Finally, the fabricated device was characterized in an ambient atmosphere with Keithley 4200 semiconductor parameter analyzer. Fabricated OFETs by using interdigitated bottom contact-top gate geometry was given in Fig. 1.

3. Results and discussion

3.1. Synthesis and characterization

Synthesis methods of the compounds **1a-c and 2a-c** are shown in Scheme 1. Commercially available 2-benzylphenol was used as a starting compound. The phthalonitrile derivatives (**1** and **2**) were prepared by the aromatic nucleophilic substitution reaction between 4-nitrophthalonitrile for **1** and 3-nitrophthalonitrile for **2** with 2-benzylphenol in the presence of anhydrous potassium carbonate in *N*,*N*-dimethylformamide at 65 °C under argon atmosphere. The phthalonitrile derivatives were purified by column chromatography using DCM as eluent. The cyclotetramerization of these phthalonitrile derivatives into metallophthalocyanines was accomplished with cobalt, copper, and nickel salts in a Schlenk tube at 160 °C in DMAE under vacuum. After well-purification, these novel compounds were characterized by ^{1}H NMR (for phthalonitrile derivatives), ^{13}C NMR (for phthalonitrile derivatives), UV–Vis, FT-IR, MALDI-TOF mass-spectroscopy, and elemental analysis results.

In the FT-IR spectra of 4-(2-benzylphenoxy) phthalonitrile (**1**) and 3-(2-benzylphenoxy) phthalonitrile (**2**), stretching vibration of nitrile groups were observed at 2232 and 2231 cm^{-1}, respectively. All characteristic vibration peaks (Aromatic C–H, Aliphatic C–H, Aromatic C═C, and Ar–O–Ar) of compounds **1** and **2** were observed in the FT-IR spectra of the compounds as quite clearly.

The data obtained from ^{1}H NMR spectra were in good correlation with the expected structures of synthesized 2-benzylphenoxy-phthalonitrile derivatives (**1** and **2**). In the ^{1}H NMR spectra of compounds **1** and **2**, the aromatic protons were observed in the range of 7.60–6.65 ppm. In the aliphatic region, the methylene bridge protons were observed at 3.92 and 3.98 ppm for phthalonitrile **1** and **2**, respectively. ^{13}C NMR spectra of the compounds **1** and **2** reveal 19 peaks containing 18 peaks for aromatic carbon atoms observed between 160.78 and 105.21 ppm in the aromatic region and 1 peak for methylene carbon atom at around 36 ppm.

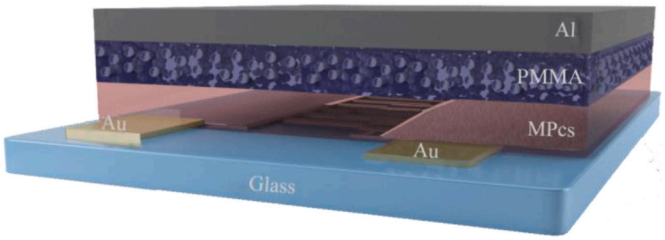

Fig. 1. Schematic structure of the bottom-contact top-gate MPcs based OFET.

In the FT-IR spectra of the phthalocyanine complexes (**1a-c and 2a-c**), the stretching vibration peaks of the nitrile groups for phthalonitriles **1** and **2** were disappeared. Similar characteristic vibration peaks (Aromatic C–H, Aliphatic C–H, Aromatic C═C, and Ar–O–Ar) were observed for the studied phthalocyanines when compared to their phthalonitrile precursors.

The UV–Vis spectra of phthalocyanine compounds (**1a-c and 2a-c**) showed monomeric behavior in dichloromethane evidenced by a single and narrow Q bands in the range of 675–683 nm for peripheral substituted phthalocyanines (**1a-c**) and 690–703 nm for non-peripheral substituted phthalocyanines (**2a-c**) (see Fig. 2). The Q-band absorptions of the phthalocyanines (**1a-c and 2a-c**) were linked to transitions from the highest occupied molecular orbital (HOMO) π levels to the lowest unoccupied molecular orbital (LUMO) π* levels. B-bands of phthalocyanines in the UV region were observed between 319 and 351 nm due to transitions from deeper π levels to the lowest empty molecular orbital (LUMO) π* levels. The energy levels of the molecular orbitals are affected by substituents in the non-peripheral part of the phthalocyanines, resulting in significant variations in the absorption spectra. Substituents in the phthalocyanine's peripheral part had a smaller impact on the Q band position. Substituents in the non-peripheral part were closer to the phthalocyanine scaffold than in the peripheral part, resulting in more a_{1u} orbital (HOMO) instability and, as a result, a larger bathochromic shift. These behaviours of B and Q bands were compatible with the literature [26–28].

In the MALDI-TOF-mass spectra using the dithranol (DIT) matrix for the phthalocyanines **1a-c**, the presence of molecular ion peaks at 1300, 1304, and 1305 confirmed the proposed structures of these compounds. On the other hand, the molecular ion peaks of non-peripheral substituted phthalocyanines **2a-c**, were obtained at 1304, 1300, and 1300. The elemental analysis results were also consistent with the structures of all synthesized compounds.

3.2. Electrochemical properties

Electrochemistry of phthalocyanine compounds (**1a-c** and **2a-c**) was investigated using the cyclic voltammetry (CV) method in DCM/tetrabutylammonium hexafluorophosphate ($TBAPF_6$) electrolyte system using a glassy carbon working electrode. The potentials were calibrated to the ferrocene redox couple $E_o(Fc/Fc^+) = +0.41$ V to determine the accurate HOMO-LUMO energy levels via oxidation and reduction potential onsets of the compounds. The oxidation and reduction potentials are summarized in Table 1.

Fig. 3 shows the CV responses of the phthalocyanine compounds in both anodic and cathodic regimes. All compounds exhibited reversible reduction potentials which are assigned to the metal center of the phthalocyanine ring. Besides, the phthalocyanine complexes indicated reversible oxidation potentials at potential values between 0.5 and 1.1 V. Unlike the other compounds, two reversible oxidation peaks were observed till 1.1 V for **1a**. Moreover, **2a** showed two reversible reduction peaks at a potential between 0 and -0.8 V according to Fig. 3. These studied phthalocyanines showed reversible redox behavior between −1.1 and + 1.1 V according to the oxidation/reduction behavior of all studied phthalocyanines. The reversible redox behavior in a narrow range is a great advantage for organic electronic applications.

Electrochemical bandgap ($E_{gap,\ electrochem}$) values of the compounds were determined from the difference between oxidation and reduction onset potentials. In addition, the optical band gap ($E_{gap,\ optical}$) was calculated from the absorption edges of the compounds. Table 1 shows

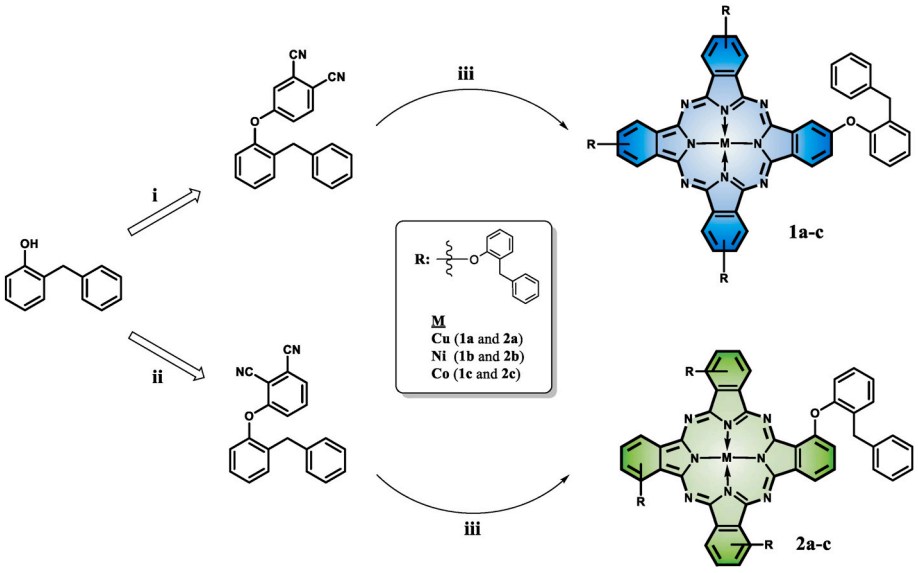

Scheme 1. Synthesis of benzylphenoxy substituted phthalonitriles and their metallophthalocyanine complexes; (i) 4-nitrophthalonitrile, DMF, K_2CO_3, rt; (ii) 3-nitrophthalonitrile, DMF, K_2CO_3, rt; (iii) DMAE, Metal salts [$CuCl_2$, $CoCl_2$, $NiCl_2$], 160 °C.

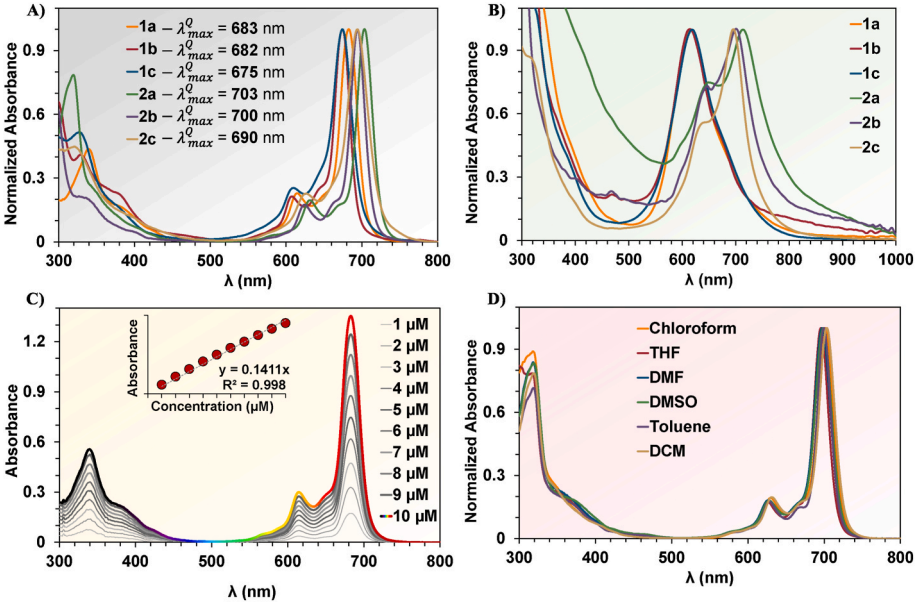

Fig. 2. Comparison of the normalized absorption spectra of the synthesized phthalocyanines (**1a-c**, **2a-c**) in dichloromethane solution (A) and on thin-film (B). Absorption spectra of phthalocyanine **1a** at different concentrations (1–10 μM) in dichloromethane (C). Absorption spectra of phthalocyanine **2a** in different solvents (D).

that the optical band gap values are higher than the electrochemical bandgap (Eg) values. This can be due to optical and electrochemical centers behaving independently from each other. Considering the charge densities of the HOMO-LUMOs in the DFT calculations, the charge distribution between the metal center and the ligand supports this situation.

3.3. Thermal properties

In an application, it is necessary to know the thermal properties of the substances to be used as materials. The thermal stability of the metallophthalocyanines containing benzyl phenoxy (**1a-c** and **2a-c**) was determined by thermogravimetric analysis (TGA) (see Fig. 4) measurements were recorded at a rate of 10 °C per minute from +25 to +900 °C in an N_2envirpment. Looking at the decomposition temperature in the first region, the composition of peripheral nickel phthalocyanine (**1b**) began to degrade at a very low temperature compared to other studied phthalocyanine compounds. The largest mass loss in the first region was observed in non-peripheral cobalt phthalocyanine (**1c**). In the non-peripheral nickel phthalocyanine compound (**2b**), a linear decrease was seen in the first region, and the peak was not calculated, it was calculated in the second region. A single peak was observed in the peripheral cobalt phthalocyanine (**1c**), while the peak observed in the second region for the non-peripheral copper phthalocyanine (**2a**) is very ineffective.

From all these results, it is observed that the thermal stabilities of the metal phthalocyanines carrying the benzyl phenoxy groups (**1a-c** and **2a-c**) are above 300 °C on average. The most stable thermal

Table 1
Cyclic voltammetry data, electrochemical and optical band gap energy $E_{gap,\ electrochem}$, $E_{gap,\ optical}$, HOMO, and LUMO values of compounds.

Pcs	Oxidation Peak Potential (V)		Reduction Peak Potential (V)		HOMO (eV)	LUMO (eV)	Egap, electrochemical (eV)	Egap, optical (eV)
1a	$E^{ox1}_{m,a} = 0.71$	$E^{ox2}_{m,a} = 0.91$	$E^{red}_{m,a} = -0.79$		−3.63	−4.80	1.17	1.56
	$E^{ox1}_{m,c} = 0.66$	$E^{ox2}_{m,c} = 0.83$	$E^{red}_{m,c} = -0.86$					
1b	$E^{ox}_{m,a} = 1.01$		$E^{red}_{m,a} = -0.83$		−3.60	−4.64	1.04	1.60
	$E^{ox}_{m,c} = 0.95$		$E^{red}_{m,c} = -0.88$					
1c	$E^{ox}_{m,a} = 0.68$		$E^{red}_{m,a} = -0.19$		−4.18	−4.65	0.47	1.57
	$E^{ox}_{m,c} = 0.57$		$E^{red}_{m,c} = -0.30$					
2a	$E^{ox}_{m,a} = 0.79$		$E^{red1}_{m,a} = -0.47$	$E^{red2}_{m,a} = -0.66$	−4.15	−4.82	0.67	1.46
	$E^{ox}_{m,c} = 0.66$		$E^{red1}_{m,c} = -0.32$	$E^{red2}_{m,c} = -0.58$				
2b	$E^{ox}_{m,a} = 0.89$		$E^{red}_{m,a} = -0.85$		−3.55	−4.82	1.27	1.54
	$E^{ox}_{m,c} = 0.65$		$E^{red}_{m,c} = -0.95$					
2c	$E^{ox}_{m,a} = 0.69$		$E^{red}_{m,a} = -0.27$		−4.08	−4.72	0.64	1.57
	$E^{ox}_{m,c} = 0.54$		$E^{red}_{m,c} = -0.41$					

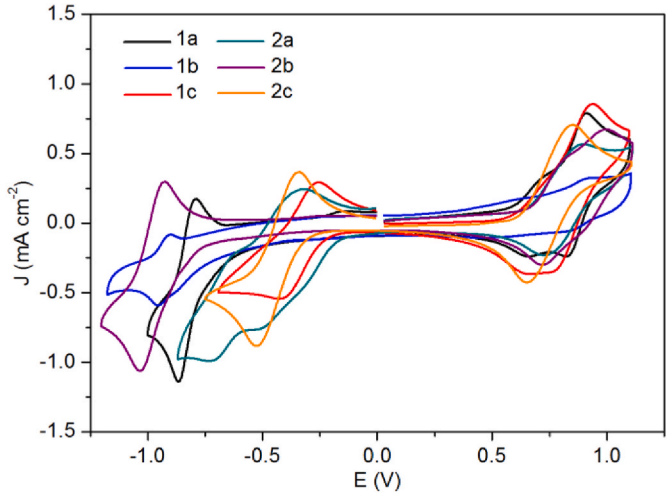

Fig. 3. Cyclic voltammograms of compounds (**1a-c**, **2a-c**) on the GCE in 0.1 M $TBAPF_6$/dichloromethane electrolyte solution at scan rate 100 mV/s vs Ag wire.

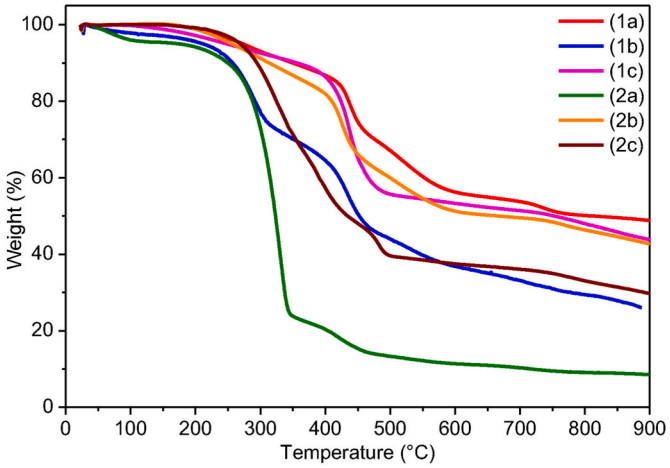

Fig. 4. TGA spectra for benzyl phenoxy-bearing metal phthalocyanines (**1a-c** and **2a-c**).

characteristic was obtained for peripheral copper phthalocyanine (**1a**) while the lowest stability was observed for peripheral nickel phthalocyanine (**1b**). Glass transition temperatures for synthesized phthalocyanines were observed in the range of 176.18–176.85 °C (Figs. S22–33). Initial decomposition temperatures, maximum decomposition temperatures, and remaining residue at 900° are given in detail on the graphics in the supporting information (Figs. S22–S33). The resistance of all synthesized phthalocyanine compounds above 300 °C shows that they are quite stable. In addition, it was determined that **1a-c**, which has a peripheral structure, showed more thermally stable than non-peripheral structures (**2a-c**).

3.4. Surface characterization

Surface characterization of drop-casted films for the studied phthalocyanines (**1a-c** and **2a-c**) was carried out via Atomic Force Microscopy (AFM) technique using tapping-mode height images. When the roughness average values of the prepared polymer films are examined, it is seen that the film roughness value for **1a** is somewhat higher than the other polymer films. Fig. 5 shows that the **1a** layer has gyroid morphology that the particles are interconnected with one another. It was observed that the position of peripheral substituent and central metal atom changed the morphology. For example, a rougher surface was observed for the copper and nickel phthalocyanine complexes (**1a** and **1b**), while a smoother surface was obtained in the thin film of the cobalt complex (**1c**). The non-uniform surface of the **1b** can be due to the planarity of the different peripheral substituents. Similar results were observed for **2a-c**. This proves that the central metal atom has a direct effect on the morphology. In addition, TEM images of all compounds were also taken as a supplement, and the crystalline morphologies of **1a**, **2a**, and **1c**, **2c** are seen in TEM images, as in AFM images (Fig. S35).

Polar materials are super hydrophilicity, while the substances above 90° are close to the hydrophobic character. The rough surfaces in the AFM show a higher contact angle. Molecules with high contact angles do not hold water. The contact angles of the copper (85.6° for **1a**, 67.8° for **2a**) and cobalt (82.3° for **1c**, 75.7° for **2c**) phthalocyanines are below 90° while the contact angles of the nickel phthalocyanines are over 90° (103.4° for **1b**, 94.9° for **2b**) and the contact angles of the cobalt phthalocyanines are below 90°. Nickel phthalocyanines are close to the hydrophobic character. Copper and cobalt phthalocyanines showed hydrophilic characters. Peripheral-substituted phthalocyanines (**1a-c**) have higher contact angles than non-peripheral phthalocyanines (**2a-c**) (Fig. S36).

3.5. Theoretical studies

Specific bond lengths and bond angles for phthalocyanines are given in Table S2. The geometry optimization parameters of the peripheral and non-peripheral cobalt, nickel, and copper phthalocyanine compounds carrying benzyl phenoxy are different from each other due to the difference of the metal in the cavity and the position of the substituents

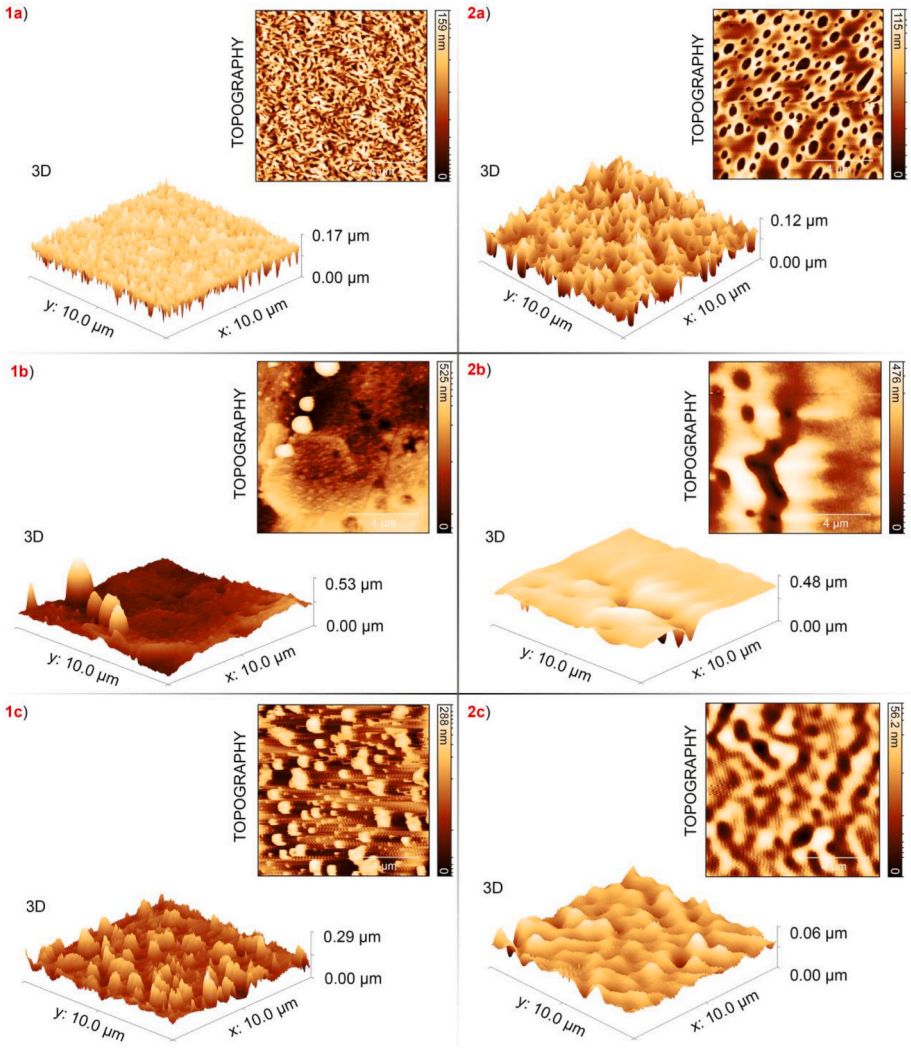

Fig. 5. AFM (tapping-mode height images) of phthalocyanines (**1a-2c**) films.

on the ring. The total energy of the system is very close to each other as they are the same for peripheral and non-peripheral phthalocyanines in terms of atomic number and type. Copper has more electrons than cobalt and nickel, and it more chemically interacts with the phthalocyanine ring. Thus, the energy level of the system for comparison is lower compared to nickel and cobalt phthalocyanine counterparts. Since nickel metal has more electrons than cobalt, it has created more interactions. As the energy of the compounds increases in the negative direction, their stability increases. Thus, the energy ranking is found as $E_{CuPc} > E_{NiPc} > E_{CoPc}$.

Metal-N bond length is different among the studied cobalt, nickel, copper phthalocyanines. In the copper phthalocyanines (**1c** and **2c**), the Metal–N bonds (1.94 Å) are shorter than the cobalt phthalocyanines (**1a** and **2a**) Metal–N bonds (1.97 Å), and longer than the nickel phthalocyanines Metal–N bonds (1.92 Å). There was no change in the bond lengths of the peripheral and non-peripheral phthalocyanines cavity and the bond lengths were measured identically. The bond lengths between the carbon of the isoindole moiety of the phthalocyanine ring and the oxygen of the benzyl phenoxy compound remained the same when the metals were changed. The O–C bond distance from the peripheral position is 1.38 Å and the O–C bond distance from the non-peripheral position is 1.37 Å. In covalent bonds, the shorter bond means it is more stable. The bond with the substituent at the non-peripheral position is more stable than the bond of the substituent at the peripheral position. The main skeleton of Cu, Ni, and Co phthalocyanines is planar. Metals are fully seated in the phthalocyanine cavity. The bond between the nitrogen and the metal atoms (N–Metal–N) is bi-directionally equal and has an angle of approximately 180° (179.94°–179.73°). It bonded with the carbon atom of the benzyl phenoxy substituent and the indoline moiety of the phthalocyanine ring at around 120.50° in the peripheral position at around 119.90° in the non-peripheral position. The direction of the benzyl phenoxy group is around 97° in the peripheral position to the planar phthalocyanine complex and around 111° in the non-peripheral position.

The highest occupied molecular orbital (HOMO) and the lowest unoccupied molecular orbital (LUMO) energies of the benzyl phenoxy containing phthalocyanines (**1a-c** and **2a-c**) were calculated in DCM (Fig. 6). The non-peripheral phthalocyanines showed narrower bandgap values compared to peripheral phthalocyanines. The reason for this is that the non-peripheral phthalocyanines have longer wavelengths of π-π* transitions. When compared to metal differences, cobalt phthalocyanines have the widest band range (−2.19 eV for **1c** and −2.12 eV for **2c**). Also, copper phthalocyanines have the narrowest bandgap (−2.13 eV for **1a** and −2.06 eV for **2a**). Since the absorptions of nickel and cobalt phthalocyanines are at the same wavelength, the bandgap is equivalent over the UV–Vis spectrum and the difference cannot be determined. Theoretical and experimental values are compatible with each other. The calculated electronic spectra of the **1a-c** and **2a-c** compounds were compared with the experimental spectra in Fig. S38, and the Q-band electronic transitions were described.

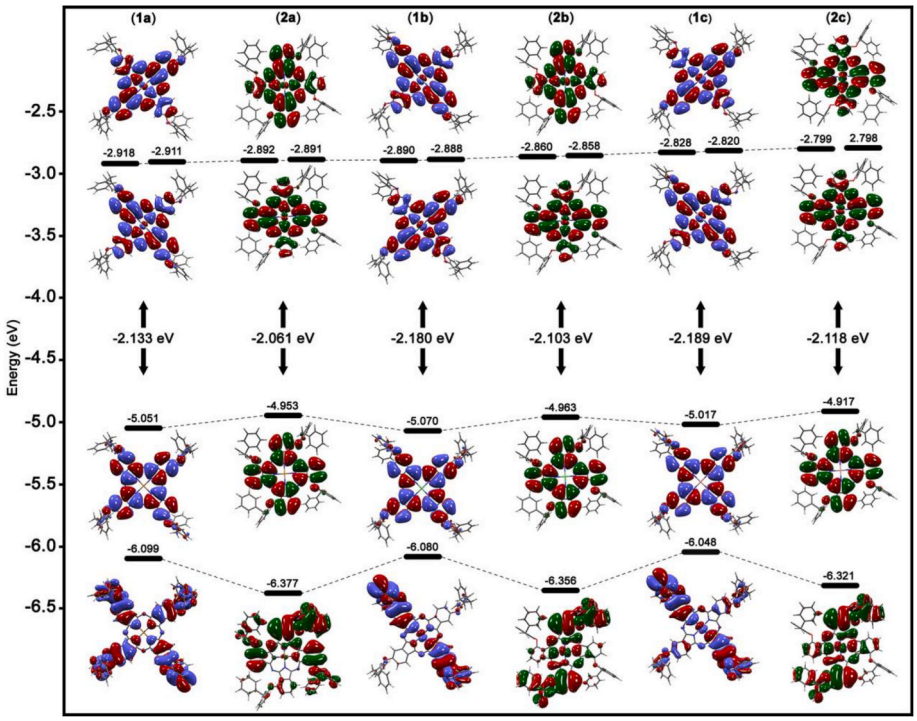

Fig. 6. The molecular orbital energy diagram of phthalocyanines (**1a-c** and **2a-c**) in dichloromethane.

The total electron density was studied in dichloromethane. Total SCF Density mapped with electrostatic potential (ESP) was used to indicate the total electron density (isoval = 0.0004 e/au^3). The red color shows the electronegative region, the green color shows the neutral region, and the blue color displays the electropositive region. The nitrogen atoms in the meso positions of the phthalocyanine compound and the oxygen atoms bridging between the Pc ring and the benzyl group are strongly electronegative due to their unpaired electrons. The inside of the benzene rings of the substituent is electronegative due to electron conjugation and its acidic aromatic and aliphatic hydrogens are electropositive. Nickel metal is more electronegative than cobalt and copper, and in nickel phthalocyanine compounds. The center of the cobalt and copper phthalocyanine compounds is either electropositive or neutral. The electronegativity order of metals is $\chi^{Ni} > \chi^{Cu} > \chi^{Co}$. The obtained results show that the HOMO-LUMO levels comply with each other when compared to the data obtained as a result of optical and electrochemical measurements. This situation is also reflected in OFET performances.

3.6. OFET characterization

MPcs molecules have shown π-π sequence. Due to overlapping

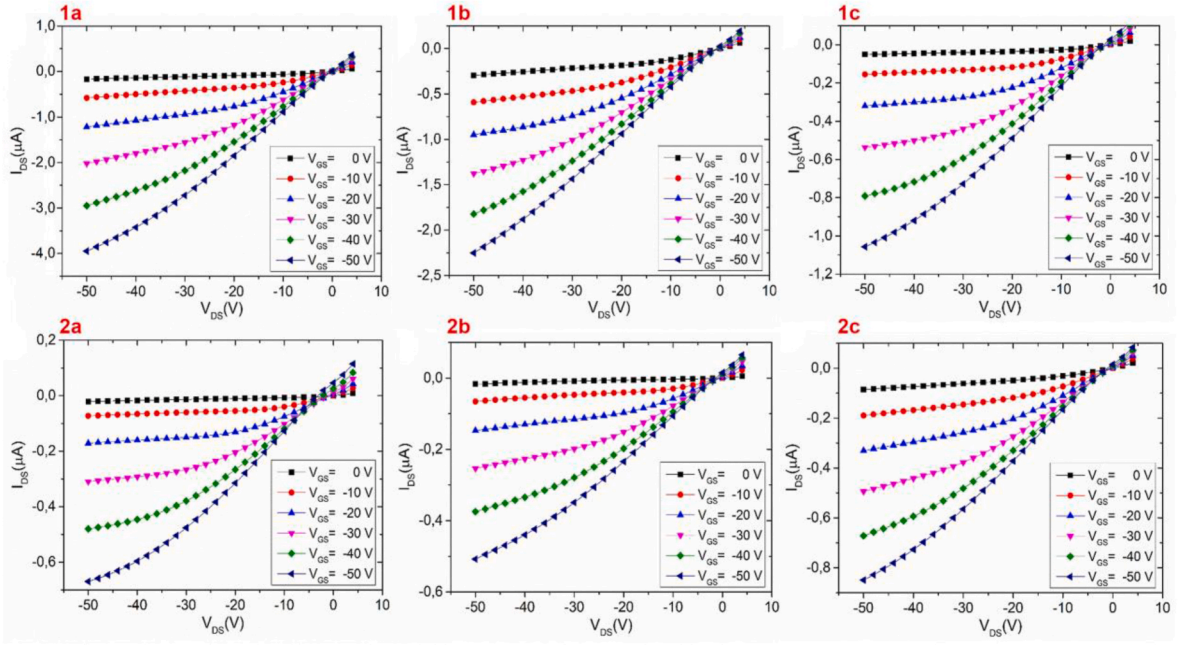

Fig. 7. The output characteristic of phthalocyanines **1a-c** and **2a-c**.

between π-orbitals of the adjacent molecule, the alignment of MPcs molecules to columnar molecular clusters is secured and one-dimensional wires are formed surrounded by an insulating layer produced by aliphatic chains. Therefore, the electrons can be shared between all the atomic centers' molecules, which can lead to an increase in carrier mobility [29,30]. Looking at the output (Fig. 7) and transfer (Fig. 8) characteristics, the curves show the behavior of the traditional phthalocyanine-based field-effect transistor. When negative bias to the gate electrode, typical behavior for hole-enhancement mode (p-type) was observed. Due to the p-type channel accumulation, it is expected that the charge injection from metal electrodes into the organic semiconductor occurs. In hole-enhancement mode, I_{DS}-V_{DS} exhibits linear region at small V_{DS} and saturation region at high V_{DS} due to the pinch of the channel.

Mono- and ball-type dinuclear Co(II), Zn(II), Cu(II) Pcs had been reported. The charge transport properties of these MPc OFETs films had been investigated as spin-coated active layers. The mobility value and threshold voltage had been found as $\mu = 4.4 \times 10^{-2}$ cm^2/Vs and 27.6 V, respectively [31]. TiOPc films have been exhibited an n-type semiconducting behavior, which their electron mobility at room temperature had 9×10^{-6} cm^2/Vs [32]. The reported Pc-based OFETs have field-effect mobilities ranging from 9×10^{-6} cm^2/Vs to 10 cm^2/Vs [33]. The mobilities have changed depending on the central metal atom, gate dielectric, and deposition techniques and parameters. It is important that Pc compounds with substituents on the ring system are essentially soluble in organic solvents and are therefore amenable to solution processing for deposition as thin films. It was found that the maximum field-effect mobility of cobalt, manganese, and zinc phthalocyanine complexes containing 4-pentylphenylethynyl substituents is 4.27×10^{-3} cm^2/Vs [34].

The electric parameters were calculated using a standard analytic theory of FET according to the following equation [35]:

$$I_{DS,\ sat} = \frac{WC_i}{2L}\mu(V_{GS} - V_{Th})^2$$

where $I_{DS,sat}$ is the saturation source-drain current, V_{Th} is the threshold voltage, V_{GS} is the gate voltage, μ is the field-effect mobility, W and L are the channel width and length, respectively, C_i is the insulator capacitance per unit area.

Table 2 shows the OFET parameters obtained from Figs. 7 and 8. As can be seen from Table 2, the peripheral and non-peripheral phthalocyanine-cobalt complexes based OFETs have higher mobility with approximately 5×10^{-2} cm^2/Vs mobility than others. It is thought that π-π stacking of phthalocyanine-cobalt complexes contributed to charge accumulation and resulted in high mobility. I_{on}/I_{off} ratio is about 10^3 - 10^4 for phthalocyanine-cobalt complexes which is quite a high value. The threshold voltage (V_{Th}), which can be caused by impurities in the semiconductor, interface states, and charge traps, is an important parameter for OFETs [36]. Subthreshold swing (S) is the inverse slope of the drain current versus the gate voltage in a semilog plot ($S = dV_{GS}/d(\log(I_{DS}))$). It is often used to characterize the subthreshold regime by indicating how rapidly the device switches from the OFF to the ON state. A large value of S generally implies a large concentration of shallow traps. Subthreshold swing has also been evaluated in order to extrapolate the maximum surface trap density (NSmax) according to the relationship NSmax≈ [(S × log(e) × q/k × T)-1]C/q, where k is the Boltzmann constant, q is the elementary charge, T is temperature, and C is the capacitance value [37]. For the phthalocyanines (**1a-c** and **2a-c**), subthreshold swing value has been measured as 390 mV/decade which resulted in 8.14×10^9 charge density. Imperfect gate dielectrics, surface conduction, bulk device transport, or a lack of semiconductor patterning can lead to gate leakage and affect the performance of many circuits. Leakage current as a function of gate voltage was as shown in Fig. S40.

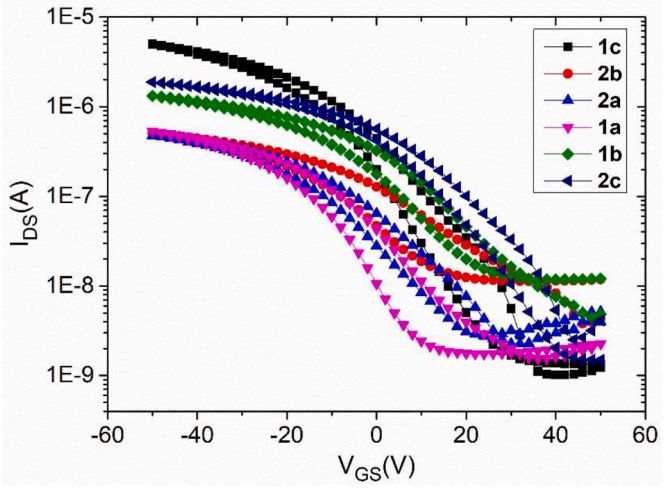

Fig. 8. Transfer characteristic of phthalocyanines (**1a-c** and **2a-c**).

Table 2
OFET parameter for the phthalocyanine (**1a-2c**).

Compound	Mobility (cm^2/Vs)	On/Off Ratio	V_{Th} (V)	I_{GS} (A)	S (V/decade)	Ns_{max}
1a	9.77×10^{-2}	10^3	11	7×10^{-9}	~0.22	5.23×10^9
2a	8.91×10^{-2}	10^3	30	9×10^{-9}	~0.23	7.46×10^9
1b	6.12×10^{-4}	10^2	57	1×10^{-8}	~0.37	1.12×10^8
2b	1.18×10^{-4}	10^2	52	1×10^{-9}	~0.39	8.14×10^9
1c	2.32×10^{-2}	10^4	35	9×10^{-9}	~0.27	1.22×10^9
2c	0.31×10^{-2}	10^3	52	1×10^{-9}	~0.28	1.41×10^9

4. Conclusion

In summary, the series of phthalocyanines based on the 2-benzylphenol substituent and cobalt, nickel, and copper as central metals in the Pc cavity were synthesized. Optical, electrochemical, spectroscopic, and theoretical results show that the HOMO-LUMO levels and a blue shift were observed for cobalt Pc complexes when compared to their counterparts. Furthermore, optical band gap values were measured at approximately 1.5 eV. The optical band gap of compounds was calculated at approximately 1.5 eV, while the electrochemical HOMO-LUMO band gap values were observed below 1.0 eV. These values are not compatible with the calculated theoretical data. This indicates that the donor and acceptor units in the compound act independently of each other. In addition, surface characterizations with AFM show that the cobalt complex **1a** has a self-organized proper distribution on the thin film surface. This has been created a positive effect on OFET results. These results show that solution-processed new 2-benzylphenoxy substituted metallophthalocyanine films can be used as a semiconductor layer of p-channel OFET devices. In the OFET measurements, it was seen that the peripheral and non-peripheral phthalocyanine-cobalt complexes based OFETs have higher mobility than other counterparts. In addition to optical and electrochemical data, OFET results have shown us that these compounds can also be used in solar cells.

CRediT authorship contribution statement

Mücahit Özdemir: Investigation, Software, Writing – original draft. **Sinem Altinisik:** Investigation, Methodology. **Baybars Köksoy:** Project administration, Writing – original draft, Preparation. **Betül Canımkurbey:** Investigation, Writing – original draft. **Sermet Koyuncu:**

Writing – review & editing, Software, Supervision. **Mahmut Durmuş:** Writing – review & editing, Data curation. **Mustafa Bulut:** Investigation, Validation. **Bahattin Yalçın:** Writing – review & editing, Supervision.

Declaration of competing interest

The authors declare that they have no known competing financial interests or personal relationships that could have appeared to influence the work reported in this paper.

Acknowledgement

The numerical calculations reported in this paper were fully performed at TUBITAK ULAKBIM, High Performance and Grid Computing Center (TRUBA resources).

Appendix A. Supplementary data

Supplementary data to this article can be found online at https://doi.org/10.1016/j.dyepig.2022.110125.

References

[1] Josefsen LB, Boyle RW. Unique diagnostic and therapeutic roles of porphyrins and phthalocyanines in photodynamic therapy, imaging and theranostics. Theranostics 2012;2(9):916. https://doi.org/10.7150/thno.4571.
[2] Allen CM, Sharman WM, Van Lier JE. Current status of phthalocyanines in the photodynamic therapy of cancer. J Porphyr Phthalocyanines 2001;5(2):161–9. https://doi.org/10.1002/jpp.324.
[3] Zysman-Colman E, Ghosh SS, Xie G, Varghese S, Chowdhury M, Sharma N, et al. Solution-processable silicon phthalocyanines in electroluminescent and photovoltaic devices. ACS Appl Mater Interfaces 2016;8(14):9247–53. https://doi.org/10.1021/acsami.5b12408.
[4] Chunder A, Pal T, Khondaker SI, Zhai L. Reduced graphene oxide/copper phthalocyanine composite and its optoelectrical properties. J Phys Chem C 2010;114(35):15129–35. https://doi.org/10.1021/jp104587n.
[5] Beneto AJ, Jeong JY, Park JS. Sub-phthalocyanine-incorporated Fe (II) metallo-supramolecular polymer exhibiting blue-to-transmissive electrochromic transition with high transmittance and coloration efficiency. Dalton Trans 2018;47(45):16036–9. https://doi.org/10.1039/C8DT03587C.
[6] Zhang X, Wang Y, Gu M, Wang M, Zhang Z, Pan W, et al. Molecular engineering of dispersed nickel phthalocyanines on carbon nanotubes for selective CO 2 reduction. Nat Energy 2020;5(9):684–92. https://doi.org/10.1038/s41560-020-0667-9.
[7] Sorokin AB. Phthalocyanine metal complexes in catalysis. Chem Rev 2013;113(10):8152–91. https://doi.org/10.1021/cr4000072.
[8] de la Escosura A, Martínez-Díaz MV, Barberá J, Torres T. Self-organization of phthalocyanine−[60] fullerene dyads in liquid crystals. J Org Chem 2008;73(4):1475–80. https://doi.org/10.1021/jo7022763.
[9] Basova T, Hassan A, Durmuş M, Gürek AG, Ahsen V. Liquid crystalline metal phthalocyanines: structural organization on the substrate surface. Coord Chem Rev 2016;310:131–53. https://doi.org/10.1016/j.ccr.2015.11.005.
[10] De Cupere V, Tant J, Viville P, Lazzaroni R, Osikowicz W, Salaneck WR, et al. Effect of interfaces on the alignment of a discotic liquid− crystalline phthalocyanine. Langmuir 2006;22(18):7798–806. https://doi.org/10.1021/la0605182.
[11] Kaya EN, Tuncel S, Basova TV, Banimuslem H, Hassan A, Gürek AG, et al. Effect of pyrene substitution on the formation and sensor properties of phthalocyanine-single walled carbon nanotube hybrids. Sens Actuators, B 2014;199:277–83. https://doi.org/10.1016/j.snb.2014.03.101.
[12] Klyamer DD, Sukhikh AS, Krasnov PO, Gromilov SA, Morozova NB, Basova TV. Thin films of tetrafluorosubstituted cobalt phthalocyanine: structure and sensor properties. Appl Surf Sci 2016;372:79–86. https://doi.org/10.1016/j.apsusc.2016.03.066.
[13] Fleischmann EK, Zentel R. Liquid-crystalline ordering as a concept in materials science: from semiconductors to stimuli-responsive devices. Angew Chem Int Ed 2013;52(34):8810–27. https://doi.org/10.1002/anie.201300371.
[14] Mason CR. Synthesis and characterisation of oligothiophenes for photovoltaic applications. United Kingdom: The University of Manchester; 2006.
[15] Zanfolim AA, Volpati D, Olivati CA, Job AE, Constantino CJ. Structural and electric-optical properties of zinc phthalocyanine evaporated thin films: temperature and thickness effects. J Phys Chem C 2010;114(28):12290–9. https://doi.org/10.1021/jp1008913.
[16] Shin EY, Cho HJ, Jung S, Yang C, Noh YY. A high-k fluorinated P (VDF-TrFE)-g-PMMA gate dielectric for high-performance flexible field-effect transistors. Adv Funct Mater 2018;28(4):1704780. https://doi.org/10.1002/adfm.201704780.
[17] McKeown NB. Phthalocyanine materials: synthesis, structure and function. Cambridge University Press; 1998.
[18] Kohn W, Sham LJ. Self-consistent equations including exchange and correlation effects. Phys Rev 1965;140(4A):A1133. https://doi.org/10.1103/PhysRev.140.A1133.
[19] Frisch MJ, Trucks GW, Schlegel HB, Scuseria GE, Robb MA, Cheeseman JR, et al. Gaussian 09, revision D.01. Wallingford CT: Gaussian, Inc.; 2013.
[20] Dennington R, Keith T, Millam J. GaussView, version 5. Shawnee mission. KS: Semichem Inc.; 2009.
[21] Becke AD. Density-functional exchange-energy approximation with correct asymptotic behavior. Phys Rev A 1988;38(6):3098. https://doi.org/10.1103/PhysRevA.38.3098.
[22] Becke AD. Becke's three parameter hybrid method using the LYP correlation functional. J Chem Phys 1993;98:5648–52. https://doi.org/10.1063/1.464913.
[23] Lee C, Yang W, Parr RG. Development of the Colle-Salvetti correlation-energy formula into a functional of the electron density. Phys Rev B 1988;37(2):785. https://doi.org/10.1103/PhysRevB.37.785.
[24] Tomasi J, Mennucci B, Cances E. The IEF version of the PCM solvation method: an overview of a new method addressed to study molecular solutes at the QM ab initio level. J Mol Struct: THEOCHEM 1999;464(1–3):211–26. https://doi.org/10.1016/S0166-1280(98)00553-3.
[25] Tomasi J, Mennucci B, Cammi R. Quantum mechanical continuum solvation models. Chem Rev 2005;105(8):2999–3094. https://doi.org/10.1021/cr9904009.
[26] Akçay HT, Menteşe E, Sökmen BB. Synthesis and spectroscopic characterization of novel methoxy bridged benzimidazolyl-substituted phthalocyanines as potent inhibitors of urease. Spectrochim Acta, Part A 2020;228:117804. https://doi.org/10.1016/j.saa.2019.117804.
[27] Keleş T, Biyiklioglu Z, Gültekin E, Bekircan O. Synthesis and electrochemical properties of peripheral, non-peripheral tetra [2-(3, 5-diphenyl-1H-1, 2, 4-triazol-1-yl) ethoxy] substituted cobalt (II), manganese (III) phthalocyanines. Inorg Chim Acta 2019;487:201–7. https://doi.org/10.1016/j.ica.2018.12.010.
[28] Akyüz D, Akçay HT, Bayrak R. Synthesis, characterization and investigation of electrochemical and spectroelectrochemical properties of peripherally tetra diethoxypropan substituted phthalocyanines. Electroanalysis 2021;33(1):146–51. https://doi.org/10.1002/elan.202060250.
[29] Borras A, Gröning O, Aguirre M, Gramm F, Gröning P. One-step dry method for the synthesis of supported single-crystalline organic nanowires formed by π-conjugated molecules. Langmuir 2010;26(8):5763–71. https://doi.org/10.1021/la1003758.
[30] Tong W, Djurišić A, Xie M, Ng A, Cheung K, Chan WK, et al. Metal phthalocyanine nanoribbons and nanowires. J Phys Chem B 2006;110(35):17406–13. https://doi.org/10.1021/jp062951q.
[31] Başak AS, Özkaya AR, Altındal A, Salih B, Şengül A, Bekaroğlu Ö. Synthesis, characterization, oxygen electrocatalysis and OFET properties of novel mono-and ball-type metallophthalocyanines. Dalton Trans 2014;43(15):5858–70. https://doi.org/10.1039/C3DT51955D.
[32] Tada H, Touda H, Takada M, Matsushige K. Quasi-intrinsic semiconducting state of titanyl-phthalocyanine films obtained under ultrahigh vacuum conditions. Appl Phys Lett 2000;76(7):873–5. https://doi.org/10.1063/1.125614.
[33] Li L, Tang Q, Li H, Yang X, Hu W, Song Y, et al. An ultra closely π-stacked organic semiconductor for high performance field-effect transistors. Adv Mater 2007;19(18):2613–7. https://doi.org/10.1002/adma.200700682.
[34] Yenilmez HY, Şahin AN, Altındal A, Bayır ZA. Photosensitive field effect transistor based on metallo-phthalocyanines containing (4-pentylphenyl) ethynyl moieties. Synth Met 2021;273:116690. https://doi.org/10.1016/j.synthmet.2020.116690.
[35] Horowitz G. Organic field-effect transistors. Adv Mater 1998;10(5):365–77. https://doi.org/10.1002/(SICI)1521-4095(199803)10:5<365::AID-ADMA365>3.0.CO;2-U.
[36] Veres J, Ogier S, Lloyd G, De Leeuw D. Gate insulators in organic field-effect transistors. Chem Mater 2004;16(23):4543–55. https://doi.org/10.1021/cm049598q.
[37] Rolland A, Richard J, Kleider J, Mencaraglia D. Electrical properties of amorphous silicon transistors and MIS-devices: comparative study of top nitride and bottom nitride configurations. J Electrochem Soc 1993;140(12):3679. https://doi.org/10.1149/1.2221149.